

## 2.4 AIRPORT TO SITE RELATIONSHIP

There are two airports in the site region, Harrisburg International Airport, formerly called Olmsted State Airport, 2.5 miles northwest, and Capital City Airport, formerly called Harrisburg-York Airport, 8 miles west northwest. The former handles primarily commercial and the latter primarily private aircraft. Runway location and use is discussed in Section 2.4.1, and the probability of airplane strikes on the plant is discussed in Section 2.4.2.

### 2.4.1 RUNWAY LOCATION AND USE

Harrisburg International Airport is located on the east bank of the river and has only one runway (130°/310°). Instrument landing approaches to 310° would align with the runway direction and the aircraft would pass approximately 7500 feet NNE of the site. Aircraft intending to land on 310° could pass near or over the site prior to turning on final approach; however, this would not be a standard VFR approach. The normal takeoff pattern on 130° is away from the site, i.e., the aircraft turns to the left after takeoff. Aircraft takeoff and landing patterns in the other respective direction are out of the site area. The missed approach holding pattern for Harrisburg International Airport is also not in the site area.

The Capital City Airport has two runways (120°/300° and 80°/260°). Instrument landing approaches to 300° would align with the runway direction and the aircraft would pass approximately 1/2 mile to the NNE of the site at an elevation of about 2300 feet. Aircraft on VFR intending to land on 300° could pass near, or over, the site prior to turning on final approach. However, 300° is seldom used due to high terrain considerations and short length (4000 feet). Occasionally, strong crosswind effects on other landing approaches require the use of this runway. Aircraft departing on 120° would normally start a right turn approximately 1 to 3 miles from the end of the runway, depending upon type of aircraft. Aircraft takeoff and landing patterns in the other respective directions are out of the site area. The Capital City Airport has one missed approach holding pattern. It is located such that aircraft would pass near the site at an altitude of roughly 3000 feet. However, aircraft in the holding pattern would comprise considerably less than 1 percent of all aircraft instrument approaches. Most aircraft having missed the landing would immediately be vectored by radar to make another approach.

## 2.4.2 PROBABILITY OF AIRPLANE STRIKES\*

### 2.4.2.1 General

The Three Mile Island Station is 2.5 miles (straight-line distance) from the eastern end of the single runway of Harrisburg International Airport. The station is about 1.5 miles to the southwest of the extended runway center line. The respective locations of the station and the airport and its runway are shown on Figure 2.4-1 of the FSAR. Air traffic patterns in the site area are based on estimates made in 1991.

Estimates of the probability of various types of airplane crashes into the plant and of related fires are given in Table 2.4-1. The development of each estimate is summarized below.

### 2.4.2.2 Probability Of Strike By Large Aircraft

Accident records in the annual statistical summaries of U.S. air carrier accidents (Reference 1) and in individual aircraft accident reports available from the National Transportation Safety Board covering about 118 million aircraft movements (landings plus takeoffs) during the 10 year period 1978 through 1987 were examined and are summarized in Tables 2.4-2, 2.4-3, and 2.4-4. This information along with data concerning the number and types of aircraft movements at Harrisburg International Airport were used to estimate the probability of a hypothetical aircraft incident as shown in Items 1 and 2 of Table 2.4-1.

The types of air carrier aircraft used in the aircraft incident study for Harrisburg International Airport in terms of approximate percent of total air carrier movements are:

DC-9	31%
Boeing 727	26%
Boeing 737	17%
Shorts 360	16%
Other	<u>10%</u>
	100%

In addition to air carrier movements, there are some Air National Guard flights from a unit stationed at Harrisburg International Airport (using C-130 and C-5A type aircraft) and some small percentage of transient military flights including helicopters. Also, United Parcel Service (UPS) began daily flights to Harrisburg International Airport using Boeing 757 in October 1989. Even though the accident records available for this study update do not go beyond 1987, this additional information has been incorporated in Section 2.4.2.3; "Probability of a strike by a very large aircraft".

\* Note: The original analyses and licensing bases can be found in the PSAR and Update-1 to the UFSAR and is based on the period of record 1956 to 1965.

Of all the aircraft using the airport, at the time of evaluation the C5A was the largest type. Table 2.4-5 gives pertinent characteristics of typical air carrier aircraft. Since most of the aircraft movements at Harrisburg International Airport are of the air carrier type, the use of air carrier accident statistics were considered appropriate.

In estimating the probability of an air carrier aircraft strike, it was assumed that there are 80,000 air carrier movements per year at Harrisburg International Airport, which was about five times the 1989 annual rate. During the 10 year period 1979 to 1988, total air carrier movements in the U.S. increased by a factor of about 37 percent. If the national increase in the next ten years is like that in the past ten and Harrisburg International Airport increases at twice that national rate, it would have about 62,000 movements per year by 1999, but would not reach 177,000 movements during the plant lifetime if movements continued to increase by the same increment each year. Even if a doubling of the movements in five to ten years is assumed and if this very fast increase were achieved and sustained, 177,000 movements per year could be realized by sometime between 1990 and 2000. Since the midpoint of assumed plant life will be about 1994, the assumption of 177,000 air carrier movements a year as a basis for statistical analysis is believed to be reasonable.

Using the data of the National Transportation Safety Board summarized in Table 2.4-2, individual accident briefs were examined to determine the portion of the total fatal accidents which occurred in the proximity of airports (i.e., within a 5 mile radius of the end of the runway being used). The results are summarized in Table 2.4-3. The types of aircraft involved in these accidents are listed in Table 2.4-4.

The accidents which involved one or more fatalities were chosen as the basis for estimating the probability of the types of crashes which could have a significant effect on the plant because the occurrence of fatalities is usually due to high deceleration rates and/or large fires. Nonfatal accidents were not included because examination of the records indicates that those occurring away from the airport runways usually have some direction and altitude control before impact and are of the type in which there is a good chance large structures could have been avoided.

Fatal landing accidents inside the area  $\pm$  0.5 mile from the runway extended centerline were excluded.

Fatal takeoff accidents within a radius of 1 mile were excluded. Fatal accidents outside a 5 mile radius were excluded on the grounds that accidents further out were not representative of the type which would affect the plant due to its proximity to the airport.

Random geographic distribution within a 4 mile radius was assumed for the fatal accidents selected as a data base. Random distribution was assumed because the actual distribution with respect to a runway in use appeared to be random.

The estimates of strike probability are based on statistics for the probability of a fatal accident per landing or takeoff for the 10 year period 1978 through 1987, inclusive. Accident statistics for the future will probably be different. However, fatal accident probability per landing and takeoff is expected to decrease in the future because of expected improvements in aircraft and engine reliability, new aircraft testing, navigation equipment and methods, pilot training, and fire control after impact. Further, Harrisburg International Airport has a long runway (8000 ft) which should contribute to the safety of landing and takeoff operations (it is about 1500 ft longer than the main runway at Washington National Airport and has a 1000 ft overrun on each end).

For the reason discussed above, it is probable that the fatal accident probability chosen for the statistical analysis is reasonable and may be conservative.

During the 10 year period 1978 - 1987, there were approximately 59 million aircraft arrivals and 59 million departures. Therefore, the applicable accident frequency ( $f$ ) is about  $4/(59 \times 10^6)$ , or  $6.8 \times 10^{-8}$  per departure and  $7/(59 \times 10^6)$ , or  $1.2 \times 10^{-7}$  per landing, considering the selection criteria aforementioned.

The probability of a crash on the station for any one landing or takeoff was taken to be the applicable accident frequency times the ratio of the "target area" of the plant to the "total area" in which the applicable accidents are assumed to happen with random distribution. These areas were estimated as follows:

- a. The "target area" for arrival (landing) accidents was assumed to be approximately the horizontal area (on the ground) which would be covered by the plant plus the shadow cast by the largest vertical cross section of the plant (excluding cooling towers) assuming light rays emanate from the plane as it approaches the plant along a line inclined 10 degrees above the horizontal. This angle was chosen as being a typical descent line for airplanes crashing on landing. (If the angle were greater, the area would be less and the probability of a strike would be less.) The area of the shadow so obtained was increased by 50 percent to account for airplanes which might crash in front of the plant and slide into it. The resulting target area for arrival accidents (here called  $A_a$ ) is about 0.0225 square miles.

- b. The "target area" for departure (takeoff) accidents was similarly estimated using a 45-degree approach angle believed typical of departure crashes. This area (here called  $A_d$ ) was estimated to be 0.0066 square miles.
- c. The "total area" for random distribution of departure accidents (here called  $A_{td}$ ) is  $\pi (4)^2 - \pi (1)^2 = 47.1$  square miles. Similarly, the "total area" for arrival accidents ( $A_{ta}$ ) is approximately  $\pi (4)^2 - \pi (0.5)^2 = 49.5$  square miles.

For any one arrival, the probability ( $P_a$ ) of hitting the plant is:

$$P_a = f_a A_d / A_{ta} = 1.2 \times 10^{-7} \times \frac{0.0225}{49.5} = 5.4 \times 10^{-11}$$

Similarly, for any one departure, the probability of hitting the plant is:

$$P_d = f_d A_d / A_{td} = 6.8 \times 10^{-8} \times 0.0066 / 47.1 = 9.5 \times 10^{-12}$$

and for both departures and arrivals the average probability is:

$$\frac{P_a + P_d}{2} = 3.2 \times 10^{-11}$$

This is equivalent to a recurrence interval of one strike every  $3.1 \times 10^{10}$  years per aircraft movement per year.

If it is assumed that there are about 177,000 aircraft movements a year at Harrisburg International Airport and that half of the takeoffs (44,250) and half the landings (44,250) are from the end of the runway nearest the plant and therefore could affect it, the chance for the plant being hit is:

$$p = 44,250 (P_a + P_d) = 44,250 (5.4 \times 10^{-11} + 9.5 \times 10^{-12}) = 2.8 \times 10^{-6}$$

This is equivalent to a recurrence interval for a crash on the plant of about once in 0.36 million years.

In estimating the effect of impact on the plant, it has been assumed that the impact speed is up to 200 knots. The fact that the speed limit in the geographical area of interest is 180 knots would indicate that the assumption of a 200 knot impact speed is reasonable.

2.4.2.3 Probability Of A Strike By A Very Large Aircraft  
( $\geq 200,000$  lb) At a High Angle ( $>60^\circ$ ) On a Critical Structure

The critical structures referred to in the title of this Subsection are those which are protected for direct strikes of large aircraft as described in Chapter 5.

Very large aircraft are taken as those having gross weights in excess of 200,000 lb during landing or takeoff operations at Harrisburg International Airport. Maximum takeoff and landing weights for typical aircraft involved are shown in Table 2.4-5. It should be noted in Table 2.4-5 that while the maximum takeoff weights of the B-720 and the B-707-12-B are more than 200,000 lb, the maximum allowable landing weight is less. Also, if aircraft are departing for a nearby destination, takeoff weights may be substantially less than the maximum because a full fuel load would not usually be carried.

It is assumed that very large aircraft comprise 3 percent of the total assumed air carrier movements at Harrisburg International Airport or  $0.03 \times 177,000 = 5310$  movements/year.

For purposes of approximation, a strike angle of  $60^\circ$  on critical building surfaces was chosen as a basis for investigation. Strike angles less than this (associated with any given weight, speed, and deceleration pattern at impact) would impose loads less than those derived from assuming a  $90^\circ$  impact such as has been done in checking structures for the effect of large aircraft strikes.

Flight path angle (relative to the horizontal) was assumed to be randomly distributed from  $0^\circ$  to  $20^\circ$  for landing accidents and  $0^\circ$  to  $90^\circ$  for takeoff accidents. The probability of a strike from selected directional quadrants was assumed to be 40 percent from a quadrant from  $300^\circ$  through north to  $30^\circ$ ; 40 percent from a quadrant from  $30^\circ$  to  $120^\circ$ ; 10 percent from  $120^\circ$  to  $210^\circ$ ; and 10 percent from  $210^\circ$  through  $300^\circ$ .

These percentages were selected by considering the plant location with respect to the airport and surrounding terrain. The horizontal angle of approach in any quadrant was assumed to be random.

The strike probability for large aircraft was taken to be  $2.8 \times 10^{-6}/\text{yr}$  based on an assumed virtual target area of  $630,000 \text{ ft}^2$  for landing and  $185,000 \text{ ft}^2$  for takeoff accidents. About 64 percent of the strike probability was due to landing and 36 percent due to takeoff accidents.

Given the information and assumptions described above, the probability of an aircraft larger than 200,000 lb striking the plant on a critical structure at an angle of greater than 60° relative to the structure surface can be estimated as follows.

For takeoff accidents, the probability of a very large airplane strike from a given quadrant is:

$$P_T = 2.8 \times 10^{-6} \times 0.03 \times 0.36 \times Q = 3.0 \times 10^{-8} Q$$

and for landing accidents it is:

$$P_L = 2.8 \times 10^{-6} \times 0.03 \times 0.64 \times Q = 5.4 \times 10^{-8} Q$$

Where Q represents the fraction of total strikes arriving from a given directional quadrant.

For takeoff and landing accidents, the probability of such a strike hitting a critical building at 60° for takeoff accidents is:

$$P_{CT} = \frac{f'A'P_T}{1.85 \times 10^5}$$

where f = the fraction of strikes which would impact at greater than 60° and A is the "virtual target area" of critical surfaces which could be hit at >60°. Similarly, for landing accidents the probability is:

$$P_{CL} = \frac{f'A'P_L}{6.3 \times 10^5}$$

Using this method, values of  $P_{CT}$  and  $P_{CL}$  were estimated for strikes on critical vertical surfaces from each quadrant and on critical horizontal surfaces from all quadrants.

The result indicates that the sum of probabilities from all quadrants is about  $1.7 \times 10^{-8}$ /yr.

#### 2.4.2.4 Probability Of Small Aircraft Strike

The amount of general aviation movements in the Harrisburg area has been estimated by reviewing information received directly from airport records. In 1989, there were a total of 124,700 landings plus takeoffs, or 62,350 landings and 62,350 takeoffs at Harrisburg area airports. Of these, about 46 percent occurred at Capital City and 54 percent at Harrisburg International Airport. Typical types of aircraft involved are Beechcraft, Piper, and Cessna. Characteristics of the largest and smallest of each aircraft of these types are given in Table 2.4-6.

Accident data for general aviation operations were obtained from the National Transportation Safety Board Annual Review Reports (Reference 22) and are given in Table 2.4-7. In 1986 and 1987, there were a total of 58,525,000 hours flown under the category of general aviation. In order to relate these data to numbers of landings and takeoffs, it is necessary to make a judgment of the average flight duration. This is assumed to be 1 hour. Thus, the assumed total number of landings plus takeoffs is  $11.7 \times 10^7$  for the years 1986 and 1987.

Of the general aviation accidents, only the fatal accidents are considered because in nonfatal accidents the pilot is assumed to have enough control to be able to avoid the plant. Some fatal accidents may also be of this type.

The ranges of interest are 2 to 3 miles for Harrisburg International Airport traffic and 7 to 8 miles for Capital City traffic. From a smooth curve fitted to the data in Table 2.4-7, the respective numbers of accidents are 60 and 15 over the 2 year period for these two ranges.

For Harrisburg International Airport operations, the probability ( $P_H$ ) of there being a fatal crash within 2 to 3 miles is as follows for any landing or takeoff operation:

$$P_H = \frac{60}{(11.7 \times 10^7)} = 0.51 \times 10^{-6}/\text{operation}$$

The projected number of landing plus takeoff operations at Harrisburg International Airport is  $0.54 (124,700) = 67,300$  per year. Thus, the probability of there being a fatal airplane crash within the 2 to 3 miles is:

$$0.51 \times 10^{-6} \times 67,300 = 0.34 \times 10^{-1}/\text{year}$$

The average "virtual target" area assumed for the plant for landing and takeoff accidents is approximately 0.015 square miles. This is  $0.95 \times 10^{-3}$  times the area within the 2 and 3 mile circles.

Thus, assuming random geographical distribution of the crashes within the 2 to 3 mile radius, the probability that a fatal crash resulting from Harrisburg International Airport operations would strike the Three Mile Island plant in any one year is:

$$P_H = 0.34 \times 10^{-1} \times 0.95 \times 10^{-3} = 0.32 \times 10^{-4}/\text{year}$$



Similarly, the probability ( $P_{C/C}$ ) of a strike by a fatal crash resulting from Capital City operations would strike the Three Mile Island plant in any one year is:

$$P_{C/C} = \frac{15}{(11.7 \times 10^7)} = 0.13 \times 10^{-6}/\text{operation}$$

The projected number of landings plus takeoffs at Harrisburg/York is 0.46 (124,700) = 57,400 per year. Thus, the probability of there being a fatal crash between 7 and 8 miles of the airport is:

$$0.13 \times 10^{-6} \times 57,400 = 0.75 \times 10^{-2}/\text{year}$$

The area between the 7 and 8 mile circles is 47.1 square miles so that the Three Mile Island plant occupies only  $0.32 \times 10^{-3}$  times this area. Thus, the probability that a fatal crash resulting from Harrisburg/York operations would strike the Three Mile Island plant in any one year is:

$$P_{C/C} = 0.75 \times 10^{-2} \times 0.32 \times 10^{-3} = 0.24 \times 10^{-5}/\text{year}$$

The combined probability (P) of the Three Mile Island plant being hit by a fatal crash in any one year is then:

$$P = P_H + P_{C/C} = 0.32 \times 10^{-4} + 0.24 \times 10^{-5} = 3.4 \times 10^{-5}/\text{year}$$

The probabilities estimated above are based on the approximate number of general aviation operations in 1989. If general aviation operations in the Harrisburg area increase by a factor of 5 on the average, during life of the plant, and if the accident rates remain the same as assumed, the probability ( $P'_s$ ) would increase by a similar factor and would be about:

$$P'_s = 2 \times 10^{-4}/\text{year}$$

#### 2.4.2.5 Probability Of Fire From An Aircraft Strike

##### a. Small Fires

As indicated in Table 2.4-7 for general aviation aircraft, about 32 percent of fatal crashes have postaccident fires. If this ratio is assumed valid for crashes on the plant, then the probability (P) of crash fires would be about:

$$P = 2 \times 10^{-4} \times 0.32 = 6.4 \times 10^{-5}/\text{year}$$

This assumes that the general aviation movement rate is five times the 1989 rate. Examination of Table 2.4-6 indicates these crashes will probably involve less than 400 gallons of fuel and average less than 100 gallons.

## b. Medium Fires

Medium fires are taken to be those wherein more than 400 but less than 3000 gallons of fuel are involved. At the present time, about 57 percent of movements at Harrisburg International Airport involve airplanes with a maximum fuel capacity of 3000 gallons, or less. If, however, it is assumed that at the time air carrier movements reach 177,000 per year, 50 percent of the airplanes involved carry less than 3000 gallons when landing or taking off, then the probability (P) of a medium fire is:

$$P = 2.8 \times 10^{-6} \times 0.5 = 1.4 \times 10^{-6}/\text{year}$$

assuming all air carrier crashes on the plant result in fires.

## c. Large Fires

Similarly, the probability (P) of large fires (where more than 3000 gallons of fuel are involved) can be estimated assuming 50 percent of air carrier operations have more than 3000 gallons aboard when landing or departing. Thus:

$$P = 2.8 \times 10^{-6} \times 0.5 = 1.4 \times 10^{-6}/\text{year}$$

Improvements in aircraft design, fire prevention systems, and fuel technology, especially for large aircraft, are expected to reduce the probability of postcrash fires in the future. By the time air traffic movement rates reach those assumed in making the probability estimates above, significant improvements should be realized. Thus, from this viewpoint, the probability of postcrash fires, especially for large aircraft, should be less than assumed.

## d. Fuel or Fires Affecting Critical Ventilation Openings

The probability of fire or fuel from a small airplane crash affecting the ventilation intake or outlet for the Control Room and other protected areas can be approximated by assuming that the "virtual target" is the area of the opening plus the area around it which could be hit and cause the opening to be subjected to fire or to liquid fuel or vapors at flammable concentrations. The openings are less than 400 ft<sup>2</sup>. For a small plane crash carrying an average of about 100 gallons of fuel, it is assumed the fuel-affected area could be about 10 ft x 50 ft or 500 ft<sup>2</sup>. This is believed to be a larger area than would be affected on the average.

The "virtual target" area assumed in deriving the probability for a small plane crash in Subsection 2.4.2.4 above is 0.015 miles<sup>2</sup> or about  $4 \times 10^5$  ft<sup>2</sup>, and the probability of a crash (at five times present traffic density) is  $2 \times 10^{-4}$ /year. The probability (P) of a strike on the ventilation openings can be estimated by multiplying this probability by the ratio of "virtual target" areas or:

$$P = 2 \times 10^{-4} \times \frac{500}{4 \times 10^5 \text{ Ft}^2} = 2.5 \times 10^{-7}/\text{Year}$$

This neglects the effect of protection afforded to the openings by structures which could intercept an approaching aircraft.

Consequently, the probability has been taken as being one half that estimated above or  $1.3 \times 10^{-7}$ /year.

To estimate the probability contribution from large aircraft (air carrier planes), the average amount of fuel carried has been assumed to be 5000 gallons, assuming that only a very few, if any, very large planes (i.e., B747's) will use Harrisburg International Airport.

The area affected by spread of fuel from the crash of an aircraft carrying 5000 gallons is assumed to be about 25 ft x 1000 ft or 25,000 ft<sup>2</sup>.

The probability (P) for arriving and departing accidents is given as  $2.8 \times 10^{-6}$ . If these are multiplied by the ratio of the "virtual target" area estimated above to the average virtual target area assumed in deriving the large plane strike probability, the result is an approximate estimate of the probability of fuel or fire from a large aircraft crash affecting critical ventilation openings. Thus,

$$P = 2.8 \times 10^{-6} \times \frac{2.5 \times 10^4}{4 \times 10^5} = 1.8 \times 10^{-7}/\text{year}$$

This also neglects the effect of protection afforded the ventilation openings by structures which could intercept the approaching aircraft. Consequently, the probability is taken to be about one half that estimated above, or  $9 \times 10^{-8}$ /year.

The combined probability (P) for large and small aircraft crashes affecting the ventilation opening is:

$$P = 2.2 \times 10^{-7}/\text{year.}$$

TABLE 2.4-1  
(Sheet 1 of 1)  
APPROXIMATE PROBABILITIES FOR AIRCRAFT CRASH EFFECTS  
ON THE THREE MILE ISLAND PLANT

	Approximate Mean Strike Probability/yr <sup>1</sup>	Approximate Recurrence Interval/yrs
1. Large aircraft on plant (see Section 2.4.2.2)	$2.8 \times 10^{-6}$	$3.6 \times 10^5$
2. Large aircraft (>200,000 lb.) at high angle (>60°) on surface of critical structures <sup>2</sup> (see Section 2.4.2.3)	$1.7 \times 10^{-8}$	$5.9 \times 10^7$
3. Small aircraft on plant (see Section 2.4.2.4)	$2 \times 10^{-4}$	$5 \times 10^3$
4. Fire from an aircraft strike on the plant (see Section 2.4.2.5)		
Small fires (<400 gal. of fuel)	$6.4 \times 10^{-5}$	$1.6 \times 10^4$
Medium fires (400-3000 gal of fuel)	$1.4 \times 10^{-6}$	$7.1 \times 10^5$
Large fires (>3000 gal of fuel)	$1.4 \times 10^{-6}$	$7.1 \times 10^5$
Fuel or fire affecting critical ventilation openings <sup>3</sup>	$2.2 \times 10^{-7}$	$4.5 \times 10^6$

<sup>1</sup> In making these approximations of strike probability, the effect of overflights has been ignored. In a region of medium air traffic overflight density this probability may be in the range of  $10^{-7}$ /yr for light aircraft and  $10^{-8}$ /yr for large aircraft if the same type of assumptions are used as in devising the probabilities in this table.

<sup>2</sup> Critical structures are those protected against strikes of large aircraft and against crash fires. They are discussed in Chapter 5 of the FSAR.

<sup>3</sup> Critical ventilation openings are protected against the effects of fuel or fire. The probability represents the chance that fuel or fire will occur in the immediate vicinity of the openings.

TABLE 2.4-2  
(Sheet 1 of 1)

SUMMARY OF U.S. AIR CARRIER ACCIDENTS (1,2)

<u>YEAR</u>	<u>TOTAL ACCIDENTS</u>	<u>FATAL ACCIDENTS</u> <sup>3</sup>
1978	22	5
1979	29	5
1980	19	1
1981	26	4
1982	20	5
1983	24	4
1984	17	1
1985	22	7
1986	24	3
1987	36	5

<sup>1</sup> From "Annual Review Aircraft Accident Data, U.S. Air Carrier Operations, calendar year 1987", National Transportation Safety Board, PB91-119693, NTSB/ARC-90/01

<sup>2</sup> All 14CFR121, 125 and 127 operations.

<sup>3</sup> Fatal accidents are those in which one or more human fatalities occurred.

TABLE 2.4-3  
(Sheet 1 of 1)

FATAL ACCIDENTS IN THE PROXIMITY OF AIRPORTS<sup>1,2</sup>  
(14CFR121, 125, 127 OPERATIONS)

<u>YEAR</u>	<u>TOTAL</u>	<u>NUMBER ARRIVING</u>	<u>DEPARTURE</u>
1978	2	2	0
1979	3	1	2
1980	0	0	0
1981	0	0	0
1982	3	1	2
1983	1	1	0
1984	0	0	0
1985	4	2	2
1986	0	0	0
1987	2	1	1
	<u>15</u>	<u>8</u>	<u>7</u>

<sup>1</sup> Source: Aircraft Accident Briefs, National Transportation Safety Board, Department of Transportation.

<sup>2</sup> Within a 5 mile radius of the end of the runway being estimated. National Transportation Safety Board started in 1982 compiling data for airport proximity based on the following three categories: on airport, on airstrip, and off airport/airstrip.

TABLE 2.4-4  
(Sheet 1 of 1)

TYPES OF AIRCRAFT INVOLVED IN THE FATAL  
ACCIDENTS LISTED IN TABLE 2.4-3<sup>1,2</sup>

<u>YEAR</u>	<u>AIRCRAFT</u>
1978	B727, B727
1979	L188C, DHC6, DC10
1980	None
1981	None
1982	B737, DC10, B727
1983	Hawker HS748
1984	None
1985	L188A, L188C, L1011, DC9
1986	None
1987	B707, DC9

<sup>1</sup> Source: Aircraft Accident Briefs, National Transportation Safety Board, Department of Transportation.

<sup>2</sup> Within a 5 mile radius of the end of the runway being estimated. National Transportation Safety Board started in 1982 compiling data for airport proximity based on the following three categories: on airport, on airstrip, and off airport/airstrip.

TABLE 2.4-5  
(Sheet 1 of 2)

CHARACTERISTICS OF TYPICAL AIR CARRIER AIRCRAFT<sup>1</sup>

TYPE	MODEL	WEIGHT <sup>2</sup>		DIMENSIONS	
		Maximum Takeoff (lb)	Maximum Landing (lb)	Wing Span	Length (Overall)
C-121		135,400			
Conv.	580	58,140	52,000	105'4"	81'6"
DC-9	30	98,000	93,400	93'5"	119'3-1/2"
F-27	J	42,000	40,000	95'2"	77'2"
B-707	331-C)	331,000	247,000	145'9"	162'11"
	320-C)	331,000			
Shorts	360	27,100	26,500	74'9-1/2"	70'9-5/8"

<sup>1</sup> Others-Not Used at Harrisburg International But in Operation in U.S.

B-737	200	107,000	97,000	93'	100'
B-727	200	169,000	148,000	108'	153'2"
B-720	B	234,000	175,000	130'10"	136'9"
B-707	120B	257,000	190,000	130'10"	145'1"
C-130	E	155,000	130,000	132'7"	97'9"
Electra (185 Orion)		128,000	91,300	99'8"	116'10"

<sup>1</sup> Other Planned for Operation in U.S.

DC-10		386,500	?	155'4"	179'8"
B-747		680,000	564,000	195'8"	231'4"
C5A (107-C)		764,500	635,850	222'8-1/2"	245'11"

<sup>1</sup> Unless otherwise noted, from Jane's All the World's Aircraft (1967-68 and 1990-91 editions).

<sup>2</sup> Weight for heaviest model.



TABLE 2.4-6  
(Sheet 1 of 1)

TYPICAL GENERAL AVIATION AIRCRAFT CHARACTERISTICS<sup>1,2</sup>

Type	<u>Piper</u>		<u>Beechcraft</u>		<u>Cessna</u>	
	<u>Cherokee</u> <u>(PA 28-180)</u>	<u>Navajo</u>	<u>Bonanza</u> <u>(V-35)</u>	<u>99</u>	<u>150</u>	<u>421</u>
Weight, lb	2400	6200	3400	10,200	1600	6800
Engines- number	1	2	1	2	1	2
Fuel	50	190	80	374	38	202
Gallons (max.)						
Type	gas	jet	gas	jet	gas	jet
Cruise Speed	152	224	210	250	123	238
Flaps down stall speed	57	77	63	-	48	87

<sup>1</sup> From Jane's All the World's Aircraft, (1967-1968 edition).

<sup>2</sup> Includes Largest and Smallest of each Type.

TABLE 2.4-7  
(Sheet 1 of 1)

GENERAL AVIATION  
TOTAL FATAL ACCIDENTS IN CONTINENTAL U.S.  
(1956-1966 Inclusive)

Phase of Operation (Estimated Distance from Airport)* <u>(miles)</u>	<u>Fatal Accidents</u>
Standing, Taxi, Takeoff, Approach or Landing (0-2)	311
Climb or Descent (2-5)	102
Maneuvering or Cruise (Beyond 5)	470
Other or not reported	<u>44</u>
<b>Total</b>	<b>927</b>
Fire after impact	296

\*Due to change in how General Aviation Accident Data is compiled, assumptions regarding estimated accident distance from airport were made to keep the methodology for this update consistent with the original FSAR.

The instrument used for this purpose is a strong motion recording system consisting of:

Two triaxial sensor units installed on the south side of the Reactor Building. One unit is attached directly to the Reactor Building base mat (elevation 281 ft), outboard of the containment wall. The second unit is attached to the Reactor Building ring girder, (elevation 455 ft). Peak reading accelerographs have been installed on the following representative Class I items to verify the seismic response determined analytically:

1. Nitrogen Manifold - Auxiliary Building elevation 331 ft.
2. 15 KVA Inverter IC - Control Building elevation 322 ft.
3. D.H. Surge Tank DE-T1A-Fuel Handling Building elevation 329 ft.

The time history of ground motion and resultant vibrating response will be recorded and stored digitally. The threshold seismic condition alarm will be energized at a preset seismic acceleration for either triaxial accelerometer. The operating basis earthquake alarm will be energized if the event exceeds a preprogrammed seismic spectra curve, based on data obtained from either triaxial accelerometer. These alarms are annunciated through audio and visual indications.

#### 5.1.3 AIRCRAFT PROTECTED STRUCTURES

Those structures that are vital to protection of the reactor coolant pressure boundary, safe shutdown of the plant, and/or contain radioactive materials are designed for the aircraft and associated loadings as specified in Appendix 5A.

The structures designed to the aircraft impact criteria are:

- a. Reactor Building
- b. Fuel Handling Building
- c. Designated portions of the Auxiliary Building (see Figure 5.1-1)
- d. Designated portions of the Intermediate Building (see Figure 5.1-1)
- e. Control Building
- f. Intake screen house and pump house
- g. Heat exchanger vault
- h. Air intake structure (below ground)
- i. Access tunnel-vault to Auxiliary Building

APPENDIX 5A

GILBERT ASSOCIATES, INC., REPORT

TO

METROPOLITAN EDISON COMPANY

ON

SUMMARY OF AIRCRAFT IMPACT DESIGN

FOR

THREE MILE ISLAND NUCLEAR STATION  
UNIT 1

This Report Contains:

25 pages of text  
7 tables  
42 figures

TABLE OF CONTENTS

<u>Section</u>	<u>Title</u>	<u>Page</u>
1	<u>INTRODUCTION</u>	5A-1
2	<u>DYNAMIC LOAD FACTORS</u>	5A-1
3	<u>ANALYSIS</u>	5A-2
3.1	<u>SHELL ANALYSIS</u>	5A-2
3.1.1	APEX OF THE DOME	5A-2
3.1.1.1	ANALYSIS FOR CASE A & B IMPACT LOADINGS	5A-3
3.1.1.1.1	STRUCTURAL RESPONSE	5A-3
3.1.1.1.2	LOCAL MATERIAL FAILURE	5A-5
3.1.1.2	ANALYSIS FOR CASE C IMPACT LOADING	5A-6
3.1.1.3	ANALYSIS FOR CASE D IMPACT LOADING	5A-8
3.1.2	DOMES TO GIRDER TRANSITION	5A-12
3.1.3	GIRDER TO CYLINDER TRANSITION (SPRING LINE)	5A-12
3.1.4	IMPACT AT GRADE	5A-13
3.2	<u>PLATE ANALYSIS</u>	5A-13
3.2.1	FUNDAMENTAL FREQUENCY	5A-13
3.2.2	FINITE-ELEMENT ANALYSIS FOR SLABS	5A-15
3.2.3	DESIGN CRITERIA FOR REINFORCING	5A-16
3.2.4	DESIGN CHECK	5A-16
4	<u>ADDITIONAL DETAIL STUDIES</u>	5A-17
4.1	<u>BEARING FAILURE OF CONCRETE UNDER DIRECT IMPACT</u>	5A-17
4.2	<u>SHEAR-OFF THE ANCHORS</u>	5A-18
4.2.1	CASE A: SHEAR-OFF THE ANCHORS OF VERTICAL TENDONS	5A-18

TABLE OF CONTENTS

<u>Section</u>	<u>Title</u>	<u>Page</u>
4.2.2	CASE B: SHEAR-OFF THE ANCHORS OF DOME TENDONS	5A-20
4.2.3	CASE C: SHEARING-OFF THE HOOP TENDONS	5A-21
4.3	<u>SPALLING DUE TO AIRCRAFT IMPACT ON THE OUTSIDE WALLS</u>	5A-23
4.4	<u>IMPACT EFFECTS ON EQUIPMENT AND COMPONENTS</u>	5A-24
4.5	<u>REFERENCES</u>	5A-25

LIST OF TABLES

<u>TABLE NUMBER</u>	<u>TITLE</u>	<u>PAGE</u>
5A-1	Time Variable $t_n$	5A-27
5A-2	Dynamic Load Factors (DLF)	5A-28
5A-3	Kinetic Energy of The Dome	5A-29
5A-4	Upper Bound Displacements	5A-30
5A-5	Comparison of The Stress Resultants for Prestress Loadings	5A-31
5A-6	Reactor Load (R) Calculations Case 1: With Wings and Engines Detached	5A-32
5A-7	Reactor Load (R) Calculations Case 2: With Wings and Engines Attached	5A-34

FIGURES

<u>Number</u>	<u>Title</u>	<u>Page</u>
5A-1	Total Reaction Vs Time Curve	5A.FIG-1
5A-2	Load Time Curve For 720 Aircraft At 200 Knots	5A.FIG-2
5A-3	Maximum Dynamic Load Factor Vs Period or Frequency Of A One-Degree-Freedom System Under the Impact of Boeing 720	5A.FIG-3
5A-4	Spherical Cap Under A Ring Load	5A.FIG-4
5A-5	Spacial And Time Distribution of Load On Shell	5A.FIG-5
5A-6	Grid For Dynamic Finite-Element Analysis of Aircraft Impingement on Dome	5A.FIG-6
5A-7	Effect of Aircraft Impingement On Dome of Containment Structure - Constant Deceleration	5A.FIG-7
5A-8	Deflections and Stresses For Aircraft Impingement for Time = 0.16 Seconds - Constant Deceleration	5A.FIG-8
5A-9	Velocity Diagram For 720 Aircraft at 200 Knots Impact Speed with Wings and Engines Detached	5A.FIG-9
5A-10	Velocity Diagram For 720 Aircraft at 200 Knots Impact Speed with Wings and Engines Attached	5A.FIG-10
5A-11	720 Aircraft Mass Distribution	5A.FIG-11
5A-12	Boeing - 720 Fuselage Buckling (Crushing) Load	5A.FIG-12
5A-13	Time Variation of Shell Vertical Displacements With Wings and Engines Detached	5A.FIG-13
5A-14	Time Variation of Shell Vertical Displacement, with Wings and Engines Attached	5A.FIG-14
5A-15	Time Variation of Shell Surface Stresses Aircraft with Wings and Engines Detached	5A.FIG-15



FIGURES

<u>Number</u>	<u>Title</u>	<u>Page</u>
5A-16	Time Variation of Shell Surface Stresses Aircraft with Wings and Engines Attached	5A.FIG-16
5A-17	Pressure Distribution For Aircraft Impact	5A.FIG-17
5A-18	Aircraft Impact At Girder to Dome Transition	5A.FIG-18
5A-19	Aircraft Impact At Spring Line	5A.FIG-19
5A-20	Radial Deflection Impact At Spring Line	5A.FIG-20
5A-21	Aircraft Impact At Grade	5A.FIG-21
5A-22	Rectangular Finite-Element	5A.FIG-22
5A-23	For The Roof Slab Heat Exchanger Vault Moment Diagram	5A.FIG-23
5A-24	DELETED	5A.FIG-24
5A-25	DELETED	5A.FIG-25
5A-26	Critical Aircraft Impact-Direction 1	5A.FIG-26
5A-27	Concrete Cover to Protect Against Aircraft Impact	5A.FIG-27
5A-28	Detail of Anchor Block	5A.FIG-28
5A-29	Prestress Stresses After Nine Tendons Fail	5A.FIG-29
5A-30	Critical Aircraft Impact-Directions 2 and 3	5A.FIG-30
5A-31	Equal Spacing of Roof Tendons	5A.FIG-31
5A-32	Dome Tendons	5A.FIG-32
5A-33	Minimum Spacing of Hoop Tendons	5A.FIG-33
5A-34	Comparison of Prestress Loading	5A.FIG-34
5A-35	Reaction Load and Fuselage Decel. (with Wings and Engines Detached)	5A.FIG-35

FIGURES

<u>Number</u>	<u>Title</u>	<u>Page</u>
5A-36	Reaction Load and Fuselage Decel. (with Wings and Engines Attached)	5A.FIG-36
5A-37	Hoop and Meridional Stresses at 36 Inches from the Edge of the Loaded Area	5A.FIG-37
5A-38	Average Shear Stress in the Dome at time + = 0.20 seconds. Wing and Engines Remain Attached to Fuselage	5A.FIG-38
5A-39	Average Shear Stress in the Dome at time + = 0.20 seconds. Wing and Engines Remain Detached to Fuselage	5A.FIG-39
5A-40	FEM Model - Radial Stresses Due to Prestress and Aircraft Impact	5A.FIG-40
5A-41	Radial Stresses Due to Prestress and Aircraft Impact	5A.FIG-41
5A-42	Zones in Compression or Tension Due to Prestress or Aircraft Impact	5A.FIG-42

## 1 INTRODUCTION

The vital structures of the Three Mile Island Nuclear Station Unit No. 1 as listed in Section 5.1.3 of the Final Safety Analysis Report are designed to withstand the following hypothetical aircraft impact loadings<sup>1</sup>:

<u>Case</u>	<u>Item</u>	<u>Weight</u>	<u>Velocity</u>	<u>Effective Area</u>
A	Object	6,000 lbs.	200 knots	5 ft. diameter
B	Object	4,000 lbs.	200 knots	3 ft. diameter
C	Total Aircraft	300,000 lbs.*	200 knots	16 ft. diameter
D	Total Aircraft	200,000 lbs.	200 knots	19 ft. diameter

This report presents results of the aircraft impact study, which includes the analysis of the Reactor Building shell for various locations of the above loadings; and, the plate analysis for the Case D loading, which is the basis for wall and roof slab designs for vital structures other than the Reactor Building shell. The paper entitled "On the Stress Analysis of Structures Subjected to Aircraft Impact Forces" is applicable to this work except for the static analysis of flat plates and a minor deviation in the dynamic load factors.

Also presented are additional studies to determine if the aircraft impact loading will produce a loss of prestress force in the Reactor Building shell and, if the loss of prestress does occur, what effect this loss would have on the structure.

The final study presented is concerned with the possibility of the spalling of the anchors of the liner due to an aircraft impact on the Reactor Building shell.

## 2 DYNAMIC LOAD FACTORS

The technique used to analyze these structures is based upon establishing a dynamic load factor and applying this factor to a static solution. In determining the DLF curve the response of an undamped, linear elastic one-degree-of freedom system is used.

\* The analytical check on the basis of this loading considered a uniform collapse resistance of the fuselage which indicated that the integrity of the Reactor Building would not be jeopardized. Further investigation indicated that the assumption regarding uniform deceleration is not conservative. When a revised description of deceleration for Case C was assumed, based on a variable distribution similar in principle to that shown in Figure 5A-35 for Case D, the analytical methods employed did not demonstrate that the Reactor Building would remain stable. As

described in Section 3.1.1.2, the check was made for the Case C aircraft based on a constant loading and was found to be less severe than the Case D aircraft analyzed is described in Section 3.1.1.3. Because of the extremely remote probability of the Case C aircraft impacting at the most unfavorable location and attitude, the Case D aircraft for impingement was finally adopted as the design basis.

The idealized total reaction vs time curve is as shown in Figure 5A-1. This total reaction vs time curve describes quite well the results obtained from Tables 5A-6 and 5A-7 and figures 5A-35 and 5A-36. The time variable  $t_n$  and the ratio factor for a Boeing 720 airplane (Figure 5A-1) are shown in Table 5A-1.

The equations for dynamic load factors (DLF) for an undamped linear elastic one-degree-of-freedom system<sup>2</sup> are shown in Table 5A-2 in terms of the fundamental period T. The dynamic load factor is defined as the ratio between the dynamic response at any time (t) and the static response to the peak load P.

The maximum response as a function of the period T for Boeing 720 impact is calculated by the equations of Table 5A-2 and shown graphically in Figure 5A-3. Since this maximum response curve is obtained, the analysis of plate and shell structures can now be analyzed statically once the dynamic load factor is chosen from Figure 5A-3 with reference to appropriate period T. Figure 5A-3 represents a revised curve obtained

from plotting additional points at  $\frac{5}{1000} - \frac{2}{100}$  cps frequency steps.

Basically this curve is similar to the previous one but does pick up some oscillation which has been considered in the design.

### 3 ANALYSIS

The analysis of the vital structures as defined in Section 5.1.3 of the Final Safety Analysis Report is divided into two concepts: Section 3.1, Shell Analysis; and Section 3.2, Plate Analysis of this appendix.

#### 3.1 SHELL ANALYSIS

This analysis is used for the Reactor Building. The areas of impact that are considered to be the most critical are; Apex of the Dome, Dome to Girder Transition, Girder to Cylinder Transition, Impact at Grade.

##### 3.1.1 APEX OF THE DOME

This analysis is divided into three parts.

### 3.1.1.1 Analysis For Case A & B Impact Loadings

A study of the protection against missiles resulting from a hypothetical aircraft impact was made. The hypothetical missiles are defined as follows:

<u>Case</u>	<u>Weight</u>	<u>Velocity</u>	<u>Impact Surface</u>
A	6,000 lb	200 knots	5 ft diameter
B	4,000 lb	200 knots	3 ft diameter

This study consisted of an investigation of the overall structural response due to central impact of the missile on a spherical dome as well as the resistance to penetration due to a local material failure.

#### 3.1.1.1.1 Structural Response

##### a. Introduction

An upper bound of permanent displacements was determined resulting from direct central aircraft impingement on a spherical dome. The basic tool used was the displacement bound theorem for rigid-plastic continua<sup>3</sup>. The initial velocity distribution is determined on the basis of an inelastic collision between the missile and the structure.

##### b. Limit Analysis for Ring Loads

First we considered a simply supported spherical cap under a ring load (See Figure 5A-4). The intensity of the load is "P" per unit length (i.e. the total load =  $2\pi Pa$ ). A lower bound on the limiting value of "P" is found by determining a stress field which satisfies equilibrium condition and which nowhere violates the yield condition.

To obtain a lower bound, we assumed that for  $r \geq a$

$$N_{\phi} = 0, M_{\theta} = M_0$$

where " $M_0$ " is the fully plastic moment per unit length. On this basis it can be then determined that:

$$2\pi Pa = \frac{4\pi M_0 \sin \bar{\phi}}{\cos \bar{\phi}} \frac{1}{\ln \left[ \frac{(1+\sin\alpha)(1-\sin\bar{\phi})}{(1+\sin\bar{\phi})(1-\sin\alpha)} \right]}$$

where " $2\pi Pa$ " is the total ring load.

For this condition where  $\frac{a}{R}$  approaches zero.

$$\frac{2\pi Pa}{M_0} = 1.81\pi$$

### c. Determination of the Initial Velocity Field

From the elastic solution for a concentrated load at the apex of a shell investigators have determined that " $r_e$ ," the length over which the initial velocity distribution is felt is approximately  $2\sqrt{hR}$  where " $h$ " is the shell thickness.<sup>4,5</sup> Therefore the initial velocity is sensibly zero for  $r = r_e$ .

The initial velocity distribution is considered proportional to the elastic static deflection due to a concentrated load at the apex. Because it is difficult to determine these deflections in closed form for a spherical shell it was necessary to approximate the deflection by several functions each one of which were used to determine  $\lambda M$  velocity of the missile immediately after contact. These functions included the following:

1. Linear variation
2. Simple trigonometric variation
3. Variation suggested by a simply supported circular plate under a central concentrated load.
4. Variation suggested by a clamped circular plate under a central concentrated load.

For these cases the numerical values of " $\lambda$ ",  $v_0$  and  $T_0$  are as shown on Table 5A-3.

where  $\lambda$  = fraction of responding dome mass as previously described

$v_0$  = velocity of  $\lambda M$  immediately after contact

$T_0$  = initial kinetic energy of the dome

### d. Application of the Displacement Bound Theorem

Using the displacement bound theorem it can be shown that

$$W_0 \text{ U.B.} = \frac{T_0}{1.81\pi M_0}$$

where  $W_0 \text{ U.B.}$  is the upper bound of the deflection at  $r = 0$ .

" $M_0$ ," the fully plastic moment per unit length, is conservatively developed considering that at plastic collapse the tendons are not carrying any load and that only the 3/8 in. steel liner acts as reinforcement with a yield strength of 30,000 psi. Therefore  $M_0 = 393,000 \text{ lb ft/ft}$  which results in a conservative lower bound. Considering the previous cases for distribution of initial velocity, the upper bound of displacements are therefore as shown on Table 5A-4.

The average value of 0.97 inches for  $W_o^{U.B.}$  is considered to be a reasonable and representative number for an upper bound deflection. It should be noted that this analysis provides only an order of magnitude determination of the upper bound of displacement and based upon comparison with actual displacement of a flat circular plate with " $a/R = 0$ ," that is a concentrated in lieu of a ring load, the upper bound errs on the high side.

The conclusion can be drawn on the basis of this analysis that the structural response of the dome does not produce a condition of collapse. This solution does not consider the problem of local material failures which could lead to a more serious problem than the overall structural response.

### 3.1.1.1.2 Local Material Failure

A study was made of the problem of local penetration making use of the modified Petry formula, wherein:

$$D = k A_p V'$$

where  $D$  = depth (in feet) of penetration

$k$  = experimentally obtained material's coefficient for penetration

$A_p$  = sectional pressure obtained by dividing the weight of the missile by its maximum cross-sectional area (expressed as pounds per square foot)

$V'$  = velocity factor expressed as  $\log_{10} \left( 1 + \frac{V^2}{215,000} \right)$

where " $V$ " represents the terminal or striking velocity in feet per second.

On the basis of " $k$ " being equal to 0.0023 the penetrations are as follows:

Case A  $D = 0.128 \text{ ft} = 1.54 \text{ in.}$

Case B  $D = 0.237 \text{ ft} = 2.85 \text{ in.}$

both of which are less than the limit established for valid use of this equation. The material coefficient " $k$ " has been determined by experimental results for reinforced concrete with different compressive strengths. Variation in material properties will affect the  $k$ -value used and thereby the depth of penetration. However, the thickness of the reinforced concrete used for aircraft protected structures exceeds the lower limit for use of the modified Petry formula. A study of missile penetration was made using the Ballistic Research Laboratories formula<sup>22</sup> which resulted in deeper penetration but well within acceptable limits.

The impact of detached aircraft elements such as engines etc., will hit at a distance away from the center of impact. The top and bottom surface of the shell (See Figure 5A-15) in this location will be in compression, and the combined flexural stress less than at the center of impact. The engines have not been considered to hit at center of impact, however, the effect of the whole Class D aircraft remaining intact has been evaluated as discussed in Section 3.1.1.3.

### 3.1.1.2 Analysis For Case C Impact Loading

A study was made of the protection against a hypothetical aircraft impingement by an aircraft weighing 300,000 pounds, traveling at a velocity of 200 knots and impacting over an area with an effective diameter of 16 feet. The stability of the reactor containment structure was verified by means of dynamic elastic analyses for the impingement of the total aircraft.

The effect of a large aircraft impingement against the apex of the reinforced concrete dome was studied by calculating the dynamic response of an elastic solid of revolution to time-dependent forces acting on the area of impact, as shown in Figure 5A-5. The magnitude and duration of the impact forces were determined according to the mass, structural characteristics, and vertical component of the velocity of the aircraft. The grid for the finite-element idealization of the dome is given in Figure 5A-6. Based on virtual work, the equilibrium equations for the entire structure are formulated as follows:

$$\ddot{\vec{d}} + [\alpha(k) + 2\beta(m)] \dot{\vec{d}} + (k) \vec{d} = f$$

where:

$(m)$  = mass matrix

$\alpha(k) + 2\beta(m)$  = damping matrix

$(k)$  = stiffness matrix

$\vec{d}$  = displacement vector

Dots indicate time derivatives. These equations are integrated by means of a Predictor-Corrector method with a Runge-Kutta-Gill starting procedure using a computer program developed at Franklin Institute Research Laboratories. FIRL is acting as Consultant to GAI in connection with this problem.

Evaluation of the results, in conjunction with a procedure proposed by Dr. Steven Batterman and utilized in the study described herein to calculate limit (final) displacements in a rigid-perfect plastic shell will lead to safe estimates of the size and velocity of the largest aircraft that may impinge upon the containment building without jeopardizing its structural integrity.



An analysis was performed considering the following loading condition (Refer to Figure 5A-5 for nomenclature):

$$P_n = 200 \text{ psi}$$

$$t_1 = 0$$

$$t_2 = t_3 \quad 0.16 \text{ sec.}$$

The diameter of the impact area was considered to be 16 feet. In order to obtain a preliminary indication of displacements, this analysis was performed on the basis of the conservative assumption of no internal damping. Also to simplify the solution, the steel liner was not considered.

The equivalent diameter of the fuselage of the B707 type aircraft is approximately 13.3 ft. The assumed impact area is considered to be reasonably indicative of the impact area of such an aircraft considering the significant distortion which will occur to the fuselage as well as the load distribution afforded by the concrete to the middle surface of the dome.

The loading pressure of the 300,000 lb aircraft without impact would be 10.4 psi. Therefore the loading considered represents a constant deceleration of the impacting aircraft of 20g. That means that the entire aircraft remains intact and all elements decelerate at 20g. This represents an equivalent load on the fuselage of the aircraft of 5,800,000 lb, which it is estimated would result in gross collapse of the aircraft.

The analysis indicates that the maximum displacements and stresses all of which occur at the center of impact (i.e. the apex of the dome) are as follows:

	<u>Displacement (in.)</u>	<u>Stress (psi)</u>
Maximum	-0.98	-2264 + 354
Static	-0.66	-1832 + 346

The displacement at the apex of the dome as a function of time is depicted in Figure 5A-7. This graphical representation of displacements indicates that the most severe duration of the loading is equal to or greater than 0.16 seconds. The static displacement is that produced

by the 200 psi loading applied for an infinite period. Figure 5A-8 depicts the displacements and stresses which occur at time 0.16 seconds after impact which is the instant of maximum displacement at the dome apex.

The loading considered in this analysis represents the case where the aircraft with all its engines, fuel tanks, and wings remains intact and the total resulting load is applied on the nose of the aircraft. It has been concluded that the resultant load due to one or both wings shearing off the fuselage and impacting against the dome will result in a less critical condition than that previously considered. The static displacement of the dome at the point of impact of one engine is approximately 0.1 inches. The displacement results from a loading equivalent to a 20g deceleration applied for an infinite period. The physical separation of engines is sufficient to produce only a minimal increase in displacements due to the fact that the wings or engines upon separation from the remainder of the aircraft would be traveling at significantly reduced speed.

The results obtained from the Analysis for Case C Impact Loading were not used for the final design of the Reactor Building Dome and Shell.

#### 3.1.1.3 Analysis For Case D Impact Loading

A study was made of the protection against a hypothetical aircraft impingement by an aircraft weighing 200,000 pounds, traveling at a velocity of 200 knots and impacting over an area with an effective diameter of 19 feet using the same analytical techniques described in Section 3.1.1.2 of this appendix. The final design of the Reactor Building was based upon the case D Impact Loading Analysis.

The load-time curves for the 200,000 lb. aircraft as shown on Figure 5A-2 were used as the design basis and was derived from the geometry, structure characteristics, and mass distribution of the B720 type aircraft.

Two loading cases were considered; one in which the outboard engines, wing structure, and outboard fuel are separated from the aircraft at a prescribed time following impact (Table 5A-6 and Figure 5A-2), and one in which the aircraft is assumed to remain intact after the initial impact (Table 5A-7 and Figure 5A-2).

The reaction load can be derived as follows:

Linear Impulse = Linear Momentum

$$\text{and: } -R \Delta t = \mu L \frac{[V - \Delta V]}{LM_2} - \frac{[\mu LV + \mu XV]}{LM_1}$$

$$R \Delta t = \mu L (\Delta V) + \mu X (V)$$

$$R = \mu L \frac{(\Delta V)}{\Delta t} + \frac{\mu \Delta X}{\Delta t} (V)$$

In the limit:  $R = \mu La + \mu V^2$   
 and  $\mu L = M = \text{mass of uncrushed aircraft}$   
 thus  $\mu La = Ma = P_B$  (the unbalanced force on the uncrushed portion of aircraft)

therefore:  $R = P_B + \mu V^2$

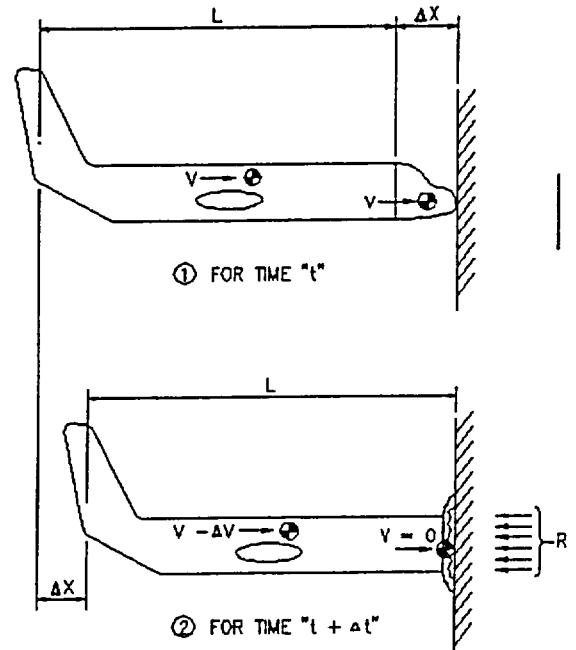
where:

$R$  = Total reaction load on rigid surface in pounds

$P_B$  = Load in pounds required to crush or deform fuselage longitudinally

$\mu$  = mass of aircraft per unit length (slugs/ft)

$V$  = velocity in ft/sec of uncrushed portion of aircraft at any time or distance during the impact



Instrumented data from a full-scale C-119 aircraft impact into a vertical wall indicated that the results given by the above momentum exchange principle for a B720 aircraft were of the right order of magnitude; however, the actual reaction load ( $P_B$ ) to the wall by the C-119 aircraft was not recorded. The rate of change of the aircraft velocity was determined, however, by high speed film analysis and compared with the rate of velocity change with the B720 aircraft as shown in Figures 5A-9 & 5A-10. This comparison shows that both aircraft decelerate at approximately the same rate; however, the B720 required more than twice as much crush distance because of its higher initial impact velocity.

The reaction load as a function of time is presented in Figure 5A-2 and 5A-35 for the B720. Note that the peak reaction occurs as the wing and fuselage are crushed between the front and rear spars. This is caused by the fact that the " $\mu^{v2}$ " is largest at this location (" $\mu$ " is very high here as shown by the mass distribution in Figure 5A-11). Also note that the fuselage deceleration is highest when the reaction load is rather low. This phenomena is caused by the reduced mass of the uncrushed portion of the aircraft being decelerated by the relatively constant buckling load ( $P_B$ ) acting on the uncrushed portion. See Tables 5A-6 and 5A-7, and Figure 5A-2. The buckling load ( $P_B$ ) of the fuselage is shown in Figure 5A-12. The average diameter of the fuselage for the B720 aircraft is 13.3 feet. As can be seen from the load-time curve the peak load occurs after the wings have impacted against the dome. Considering that the wings constitute a large proportion of the total mass, it is considered justifiable to consider a portion of the wings that is in contact with the dome at the peak load as additional impact area. Considering this additional area and the load distribution afforded by the concrete to the middle surface of the dome, the effective diameter of the impact area is 19 feet.

The analysis indicates that maximum induced extreme compressive fiber stress of 7742 psi and displacement of 1.81 inches occurs at the center of the impact area.

For the two loading cases, the displacements of the apex of the dome as a function of time are shown in Figures 5A-13 and 5A-14. For comparison, the displacement of the points at a radius of 115.2 and 268.8 inches are also shown. Stresses due to the aircraft impingement and prestress near the apex and at a radius of 85 inches are shown in Figures 5A-15 and 5A-16.

The maximum combined extreme compressive fiber stress is approximately 9372 psi. This includes stresses due to aircraft related loads and the prestress loads. It has been recognized that biaxial stress conditions as produced in the Reactor Building due to prestress, increases the ultimate strength of concrete. Considering that the minimum cylinder strength of the concrete for the Reactor Building is based upon a 28 day curing time, an increase of 20 percent in strength can be justified (Reference 12) considering that the concrete will have cured more than two years when the plant is in operation. The present records of the 90 day compressive strength of the same concrete used in the shell is in agreement with this strength increase. The strength of concrete under biaxial stress when  $\sigma_\phi \cong \sigma_\theta$  was determined by Rosenthal and Glucklich (Reference 26) to be  $2.2f'_c = 2.2 \times 6000 = 13,200$  psi.

---

\* Structural properties of the aircraft considered in Reference 1 were obtained from The Boeing Company

The local radial tensile stresses around the dome tendon conduit was determined utilizing the Finite Element Method including in the model in the effect of the 5"  $\phi$ , Schedule 40 steel tendon conduit. The model shown in Figure 5A-40 consist of an axisymmetric solid of revolution. The loads applied to the model are:

- a. Radial prestress from each of the three tendon layers
- b. Meridional prestress
- c. Meridional stresses due to aircraft impact

The resulting radial tensile or compressive stresses are shown on Figure 5A-41. The radial stresses shown in parenthesis are the results of the loads described above excluding the external dome pressure due to the crushed fuselage. The radial stresses have been adjusted for this external pressure. The stress concentration around the conduit was greatly absorbed by the steel conduit and thereby reduced the expected larger tensile and compressive stresses in the adjacent concrete. Two local areas of concrete tensile stresses exist on an axis  $45^\circ$  from the axis parallel with the dome surface. Any tensile cracking in this region would be limited by the confining compressive stresses. A local tensile crack in these regions of the concrete close to the conduit will increase the biaxial concrete compressive stress to approximately 9,150 psi < 13,200 psi considering an average stress over the uncracked portion of concrete. This is the worst condition which exists approximately 8 inches from the dome surface, and is a conservative method for evaluating the load carrying capability of the concrete. In fact, essentially all concrete is subjected to triaxial compressive stresses which further increases the concrete capacity. A schematic showing the stress state of the dome in relationship to the conduit is shown in Figure 5A-42.

The maximum compressive stress at the center of the first tendon conduit is  $f_c = 5000$  psi, with no radial tensile stresses.

The loading considered in this analysis of the dome were:

- a. Prestress load
- b. Radial tensile stresses due to tendon curvature
- c. Stresses introduced due to aircraft impact.

Stresses in the dome at the edge of the loaded area of the aircraft are for wings and engines attached:

	<u>Meridional</u>		<u>Hoop</u>
$f_c$ top	= - 6268 psi	$f_c$ top	= -6419 psi
$f_c$ bottom	= - 4931 psi	$f_c$ bottom	= +128 psi
Shear $v_c$	= 470 psi		

The concrete compressive stresses are acceptable; and the shear stress below that permitted by ACI 318-63, Chapter 26.

Stresses in the dome 36 inches out from the loaded area of the crushed aircraft for wings and engines attached (Figure 5A-37) are:

	<u>Meridional</u>	<u>Hoop</u>
$f_c$ top	= -3600 psi	$f_c$ top = -5268 psi
$f_c$ bottom	= -3440 psi	$f_c$ bottom = -342 psi
Shear $v_c$	= 356 psi	

The concrete compressive stresses are acceptable; and the shear stress below that presented by ACI 318-63, Chapter 26. (Figures 5A-38 and 5A-39)

It is of interest to note that the high fiber stresses at the apex of the dome are reduced significantly to the location at the periphery of the loaded area and at a distance "d" from the periphery of the loaded area.

No special investigation has been made for the case of simultaneous impact of the partially disabled aircraft and the detached elements (outboard engines, wing structure, and outboard fuel) on separate locations. The impact of the aircraft with a 19 ft-0 in. diameter impact area is the most critical load case. It will be seen by inspection of Figure 5A-15 that detached elements will impact in areas at significantly lower stress level. It is considered improbable that the partially disabled aircraft can impact on the structures at a location that has been damaged by the previous impact of the detached elements. The impact of the entire aircraft on the dome has been analyzed and the results are shown in Figure 5A-16.

Therefore, the conclusion can be safely drawn that the dome will not collapse due to the established loading condition.

### 3.1.2 DOME TO GIRDER TRANSITION

This analysis is in accordance with the methods described in Section 5.2.4.1 and was made for Case D loading by a hypothetical aircraft described in Section 3.1.1.3. The non-axisymmetrical load is represented by a Fourier Series and has the general dimensions and shape as shown in Figure 5A-17. The stress resultants are shown in Figure 5A-18.

### 3.1.3 GIRDER TO CYLINDER TRANSITION (SPRING LINE)

Analyzed the same as 3.1.2 above. The stress resultants are as shown in Figures 5A-19 and 5A-20.

### 3.1.4 IMPACT AT GRADE

Analyzed the same as 3.1.2. The stress resultants are as shown in Figure 5A-21.

## 3.2 PLATE ANALYSIS

This analysis was made for the Case D loading by a hypothetical aircraft as described in Section 3.1.1.3.

### 3.2.1 FUNDAMENTAL FREQUENCY

It is readily seen in Figure 5A-3 that as long as the fundamental frequency of the plate is greater than 10 cps, or less than 6 cps, the dynamic load factor will be less than 1.32. In the present plate analysis, all of the slabs have the fundamental frequency greater than 10 cps. The fundamental frequency calculated for each slab (except two slabs which will be explained subsequently) is based on the assumption of simply-supported boundary conditions. This assumption will lead to a lower value of fundamental frequency for the current plates because their boundaries are actually restrained rather than simply-supported. The value of E employed in the dynamic analyses was equal to the static modulus, and no account was taken of the increase in E resulting from the dynamic load effect in order to compensate for any reduction of E due to high stress levels. This approach is felt to be conservative because (1) the structure fundamental frequencies fall to the left of the peak in the maximum DLF vs. frequency curve and (2) the area of impact, where the highest stress levels occur, is relatively small compared with the total structure. These low values of fundamental frequency will give a conservative dynamic load factor as can be seen in Figure 5A-3. Consequently, variation of the elastic properties and edge conditions from the assumed parameters would lead to a reduction of the magnitude of the dynamic response. When the dynamic load factor value falls below unity, a minimum factor of 1.0 is used. The theoretical background of calculating fundamental frequency of simply supported plate is straightforward and well documented. (References 2, 13, and 14). The well known formula of natural frequency is:

$$\omega_{mn} = \pi^2 \sqrt{\frac{D}{\rho h} \left[ \left(\frac{m}{a}\right)^2 + \left(\frac{n}{b}\right)^2 \right]}$$

where m and n denote the mode number; D is the flexural rigidity;  $\rho$  is the density; and a, b, and h, are length, width, and thickness of plate, respectively.

For the two exceptional plates where the boundary conditions are more likely to be fixed, the fundamental frequencies are calculated based on fixed boundaries. There is no exact solution of fundamental frequency for such cases; however, numerical approximations which are based on energy principle are available. (References 2, 15, and 16). The present calculations of fundamental frequency of fixed plate are obtained from the tables and suggested formulae in Chapter 5 of "Introduction to Structural Dynamics" (Reference 2).

After obtaining the fundamental frequency of each slab and the dynamic load factor, the remaining work is a statical slab analysis. This approximate dynamic analysis technique is equivalent to the assumption that the DLF's of all modes are equal to that of the fundamental mode. For the computation of maximum response for design purposes, this approach is conservative for the following reasons:

- a. The fundamental periods of all the slabs fall to the left of the peak in the diagram of maximum DLF vs. period, thus indicating that the higher modes have smaller maximum DLF's.
- b. The maximum DLF's of the various modes do not occur simultaneously.
- c. The maximum bending moment results when the impact occurs at the center of the slab. For this case, the fundamental mode dominates the response.
- d. The maximum transverse shear is obtained when the impact takes place near a supporting edge, in which case most of the load is transferred directly to the support with little dynamic participation of the slab.

In order to assess the validity of these assertions, the study reported in Reference 21 was recently extended to evaluate the dynamic response of a typical slab subject to impact at various locations (center, edge, and intermediate points). In this study, mode superposition, using up to 900 modes (30 harmonics in each coordinate direction), was employed with the expressions for the DLF given in Table 5A-2 to calculate the time history of the displacements and stress resultants at critical positions for the Boeing 720 impact. The maximum values of these quantities were compared with the corresponding static values, and it was found that for every one the ratio of maximum dynamic value to static value was less than the maximum DLF for the fundamental mode. Therefore, the design values obtained by factoring the static responses by the maximum fundamental DLF would in every case be larger than the actual maximum, indicating that this procedure will yield a conservative design.



### 3.2.2 FINITE-ELEMENT ANALYSIS FOR SLABS

The present finite-element analysis is based upon a rectangular plate element (Figure 5A-22) as developed in References 5A-16 and 5A-17. Each nodal point has 6 degrees-of-freedom. A comprehensive explanation of the satisfaction of the "completeness" and "compatibility" of the chosen displacement function is given in References 5A-18 and 5A-19. The convergence of the solution accuracy vs grid refinement is monotonic and rapid as evidenced in various References 5A-16, 5A-17, 5A-18, and 5A-19. For the problem of plate in bending, 16 elements discretization can lead the solution of deflections to a small error of less than five percent as compared with classical solutions. The element number used in the present calculation ranges from 25 to 64 for various slabs.

Since the finite-element method is much less restricted to the geometry and boundary conditions than the classical solution, the actual geometry and boundary conditions are represented in the present calculation without modifications.

As an illustration of the present slab analysis and design, an example of roof slab at the heat exchanger vault of the auxiliary building at Elevation 305 ft is chosen. The dimensions and boundary conditions are shown in Figure 5A-23(a). The dynamic load factor, based on the elastic undamped one degree-of-freedom assumptions, was found to be 1.188.

As shown in Figure 5A-23(a), nine critical impact positions, which produce the critical moments and shears at various sections, were examined. As a simplified demonstration, the moment diagrams along line AA are shown in Figure 5A-23(b). The top and bottom reinforcements corresponding to the moments in Figure 5A-23(b) were designed and shown on GAI Drawing 422030. The shear reinforcement designed for this slab is shown on GAI Drawing 422031. The shear reinforcements were designed on the basis of the aforementioned finite-element computer program output of shears.

The slab is a rectangle 121'-0 by 55'-0 by 6'-0 as shown on GAI Drawings 422030 and 422031. The slab is supported along all four edges and along the East-West centerline. For the purpose of this analysis, only the southern half has been considered. Moment curves have been plotted for the different impact positions. Five impact positions have been considered. An envelope was then constructed in order to obtain maximum moments at any point along section A-A, Figure 5A-23. This envelope was used to calculate the required reinforcement. A similar procedure was used to calculate the moments for another 4 strips of the slab in the North-South direction and 5 strips in the East-West direction.

### 3.2.3 DESIGN CRITERIA FOR REINFORCING

The wall and roof slabs exposed to aircraft impact have been designed according to the following criteria.

- a. The main reinforcing is designed on the basis of bending moment diagrams obtained from computer printouts using Case D loading and according to the ACI 318-63, Ultimate Strength Design Method, Chapter 15.
- b. The shear reinforcing is designed on the basis of the shear force diagram obtained from computer print-outs using the Case D loading and according to the ACI 318-63, Ultimate Strength Design Method, Chapter 17.
- c. Anchorage for the reinforcing bars is provided by carrying the reinforcing bars past the theoretical cut-off point a distance sufficient to develop the ultimate strength of the bar.
- d. The allowable bond stresses are calculated on the basis of ACI 318-63, Chapter 18.
- e. No welding has been done on reinforcing bars.
- f. In the design no special construction methods were specified.

### 3.2.4 DESIGN CHECK

It is recognized that the elastic analysis employed for the flat slabs is conservative and that the resulting design does have a capacity in excess of that implied by the load considered for slab design.

As a conclusion of this design, each wall and roof slab exposed to aircraft impact was checked utilizing the Yield Line Theory (Reference 25).

These aircraft-protected structures can withstand at least a load equal to  $1.52 \times (17,500,000) = 26,400,000$  lbs. This load represents the maximum load as determined in the previous section, with the peak DLF = 1.52 as shown in Figure 5A-3.

#### 4. ADDITIONAL DETAIL STUDIES

Some additional studies on the detail structural analysis of the aircraft impact on the containment vessel have been made:

- a. Bearing failure of concrete in the neighborhood of anchors of tendons under direct impact.
- b. Shear-off of the anchors of the dome tendons, vertical tendons, and hoop tendons.
- c. Spalling due to aircraft impact on the outside wall.
- d. Impact effects on equipment and components.

##### 4.1 BEARING FAILURE OF CONCRETE UNDER DIRECT IMPACT

The bearing capacity of concrete, according to ACI-318-63, is  $1.9 \times 0.375 f'_c = 3560$  psi. The aircraft impact force of 21,100 kips (assuming a dynamic load factor of 1.2), according to the 19 foot diameter (283.5 ft<sup>2</sup>) circular normal impact area, produces an impact pressure of  $21.1 \times 10^6 / 283.5 \times 144 = 517$  psi. It is readily seen that the aircraft impact does not cause bearing failure as long as the total impact force is distributed on an area greater than 41.1 ft<sup>2</sup>. (Reference 2) (corresponding to a bearing stress of 3560 psi). Thus, it may be concluded that bearing failure can be prevented as long as the impact force is distributed on an area greater than  $\frac{41.1}{283.5} = 14.5$  percent of the normal impact area.

Intuitively, it is believed that no matter where the aircraft hits, the impact area should be at least 14.5 percent of the area of the case when the aircraft impacts on a flat wall

The anchors of the dome and vertical tendons are embedded in concrete at least one foot in depth. No damage of the anchors is possible when the aircraft hits normal to the anchorages

Although the hoop tendon anchorages are not embedded in concrete, the aircraft would have to hit in a tangential direction to the containment vessel to produce a bearing failure of the anchorage.

This being the case, it is unlikely that the total impact force will be concentrated over less than 14.5 percent of the normal impact area; therefore, a bearing failure of the concrete at the hoop tendon anchorages will not occur.

## 4.2 SHEAR-OFF THE ANCHORS

Three cases have to be investigated when considering the possibility of shearing-off the anchors of the tendons due to aircraft impact, particularly the impact of engines and sharp object.

### 4.2.1 CASE A: SHEAR-OFF THE ANCHORS OF VERTICAL TENDONS

The aircraft may travel in the direction shown in Figure 5A-26 such that the anchors of vertical tendons may be sheared-off. Based on the investigation conducted in Reference 1, the information is available that the maximum response of statically equivalent impact load is  $21.1 \times 10^6$  lb (assuming conservatively a dynamic load factor of 1.2) and the maximum impact area is a 19 ft diameter circle (assuming the aircraft strikes normal to a flat wall). The shear strength at Section A-A shown in Figure 5A-27 governs whether or not the aircraft will shear the concrete and impinge at the anchors. The shear stress at Section A-A must be calculated for the worst condition of impact loading and compared with the shear capacity.

Considering the maximum aircraft impact area with a diameter of 19 ft, the maximum number of covered tendons are:

$$N = \frac{19 \text{ ft}}{\text{C. to C. dist. between anchors}} = \frac{19 \times 12}{30.5} = 7.47$$

As a very conservative estimation, the impact force on the area between two anchor centers is:

$$P = \frac{\text{Max. response}}{N} = \frac{21.1 \times 10^6}{7.47} = 2.83 \times 10^6 \text{ lb/tendon}$$

The area available for resisting the shear can be estimated from Figures 5A-27 and 5A-28

$$A = 28" \times 30.5" = 853 \text{ sq in.}$$

It is reasonable to assume that the load applied above Section A-A is proportional to the area of impact.  $\frac{[d \times 25]}{15 \times 25} 21.1 \times 10^6$  lbs.  
where  $d = 2'-2"$ .

The applied load =  $3.1 \times 10^6$  lbs which results in a shearing stress across Section A-A equal to  $\frac{3.1 \times 10^6 \text{ lbs.}}{25 (12) 28} = 369 \text{ psi} < 600 \text{ psi}$

Ultimate shear strength of concrete  $f_{ult} = 600$  psi. Although unlikely, it is, however, assumed that nine anchors are sheared-off by the aircraft impact. As illustrated in Figure 5A-29(a) it is seen that Section AA is of primary concern if vertical tendons fail under the impact. The moment  $m_1$ , caused by the aircraft impact, has to be resisted by the moment  $m_2$ . The moment caused by the aircraft impact is:

$$m_1 = 21.1 \times 10^3 \times 166.5 \times 12 = 4.2 \times 10^7 \text{ in-kips}$$

The moment due to the undestroyed tendon prestressed forces resisting,  $m_2$  is:

$$m_2 = T(d_1 + d_2)$$

where  $T$  is the total prestressed forces on tension side of N.A., for the case when there is no tensile force in section AA. The tendons do not exceed their prestressed forces. Then,

$$T = 37 \times 2 \times 1090 = 8.06 \times 10^4 \text{ kips}$$

$d_1$  and  $d_2$  are the distances from the neutral axis to the centers of gravity of the active tendons on the tension and compression sides of the neutral axis respectively as shown in Figure 5A-29(b). Therefore:

$$m_2 = T(d_1 + d_2) = 8.06 \times 10^4 \times 987 = 7.95 \times 10^7 \text{ (k-in)}$$

It is now concluded that even with a dynamic load factor 1.2 and a very conservative assumption that nine tendons are covered by the airplane impact and are destroyed, the safety factor for not causing tension at section AA is:

$$S.F. = \frac{m_2}{m_1} = \frac{7.95 \times 10^7}{4.2 \times 10^7} = 1.90$$

In order to shear-off nine vertical tendon anchorages, the aircraft must impact as shown in Figure 5A-26. A reasonable assumption is that the impact load will be concentrated above the ring girder. As a conservative estimate of the resulting forces, the forces shown on Figure 5A-18 due to the aircraft impact at the girder to dome transition were used. Figure 5A-18 shows that the maximum moments and shears occur in the dome. Therefore, the resisting prestress forces in the critical dome area are not affected by a loss of vertical prestress.

The shear stresses in the wall are of concern because the allowable shear stress reduces when the meridional axial force is lost due to the failure of nine vertical tendon anchorages. The shear stresses at three locations were determined and compared with an ultimate shear stress of  $2\phi\sqrt{f_c}$  (ACI 318-63).

The three locations are:

- a. Cylinder wall to ring girder transition
- b. Base of wall
- c. Ten feet above the base of the wall  
(Haunch to typical wall transition)

Although the shear stress at location a. exceeds  $2.0 \sqrt{f_c}$ , the shear reinforcement required is less than that provided for the normal loading cases under no loss of prestress. The shear stresses at locations b. and c. are less than the ultimate shear stress.

#### 4.2.2 CASE B: SHEAR-OFF THE ANCHORS OF DOME TENDONS

If the aircraft impact occurs as shown in Direction 2 of Figure 5A-30, the shear resisting capacity of the concrete at Section AA has to be greater than the impact force so that no force will be transferred to the anchors of the roof tendons. The shear resisting area, assuming a 19 ft width of impact area is:

$$A = 19 \text{ ft} \times 6.416 \text{ ft} \times 144 = 17,554 \text{ in}^2.$$

The total shear capacity of concrete against the vertical impact is:

$$F = 600 \times 17,554 = 10.53 \times 10^6 \text{ lb}$$

which is smaller than the aircraft impact load  $21.1 \times 10^6 \text{ lb}$  (with a conservative assumed dynamic load factor 1.2).

It is reasonable to assume that the applied load is proportional to the area of impact.  $\left[ \frac{1.25 \times 19}{15 \times 19} \right] 21.1 \times 10^6 \text{ lbs.}$

The applied load =  $1.76 \times 10^6 \text{ lbs}$  which results in a shearing stress across section A-A of Figure 5A-30 =  $\frac{1.76 \times 10^6 \text{ lbs}}{19 (6.416) (144)} = 100 \text{ psi}$   
<600 psi.

Under the above analysis, the dome tendon anchorages will not fail in shear.

The dome tendons are composed of three layers lying on top of each other. Each layer is composed of parallel and equally spaced tendons (Figure 5A-31). As can be seen from Figure 5A-32, the orientation of the three layers is such that the tendons cross each other with a constant angle of 60 degrees. Since the dome tendons are so close to each other, crossing each other, and overlying each other is intuitively believed that no damage will occur to the dome even if a few tendons are assumed to be broken under the aircraft impact.

In addition to the previous logic, providing the failure of the dome tendon anchorages is caused by an aircraft impact as shown in Direction 2 of Figure 5A-30, the major portion of the impact load will be resisted by the cylindrical wall and not by the dome which has lost the prestress forces due to 8 broken dome tendons.

If the aircraft travels in the Direction 3 as shown in Figure 5A-30, it is seen that the concrete bearing failure is relatively small. Previously, a calculation has shown that as long as the actual impact area is at least 14.5 percent of the maximum theoretical impact area, no bearing failure will occur. Therefore, impact Direction 3 is of no critical concern.

#### 4.2.3 CASE C: SHEARING-OFF THE HOOP TENDONS

The aircraft may travel in the direction shown in Figure 5A-33. Since there is no concrete cover to protect the anchor, direct impact on the anchors may shear-off several tendons. As shown in Figure 5A-33 the minimum vertical spacing between anchors on one side of the buttress is 33 inches. Each hoop tendon is anchored in one buttress, then passes by the adjacent buttress, and is finally anchored in the next adjacent buttress. The aircraft impact area has a minimum depth of 19 ft which can cover seven (i.e.,  $\frac{19 \times 12}{33} = 6.9$ ) anchors of hoop tendons. If the

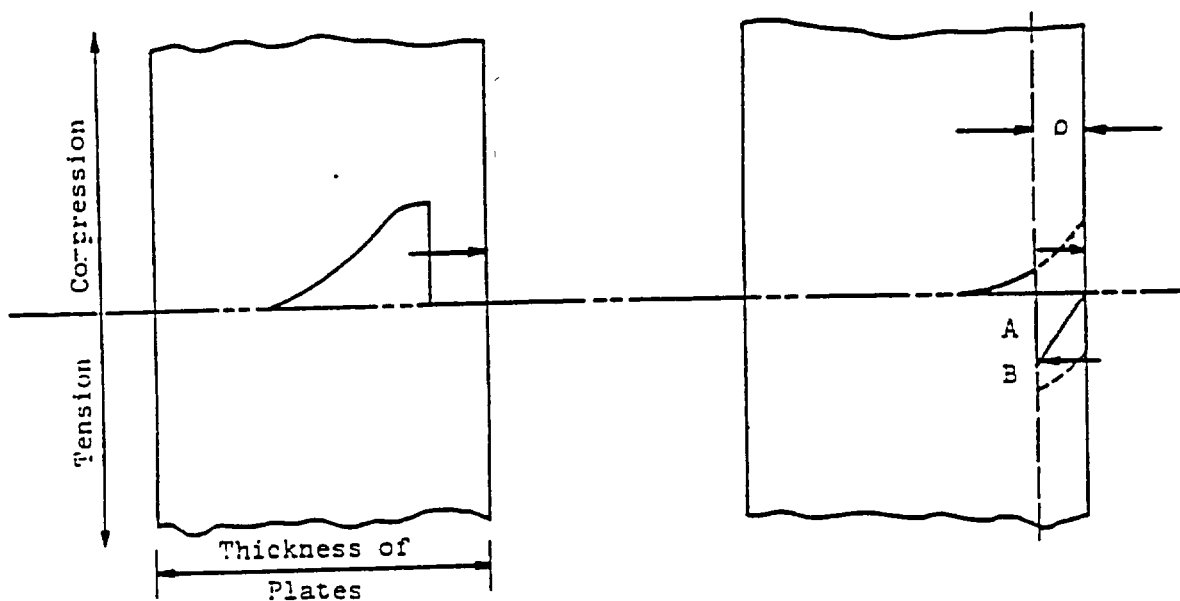
most conservative assumption is made that all of the seven anchors are sheared-off due to aircraft impact, one-half of the hoop prestress force in a cylindrical panel with a depth of 19 ft and a curve length of one third of the cylinder periphery would be eliminated. An analysis is made considering the containment vessel with normal prestress conditions with the exception that a cylindrical segment with a depth of 15 ft has only one half of the hoop prestress. The resultant axial forces and shears with half of the hoop tendon forces lost in the range between 800 inches and 965 inches above the base of the cylindrical wall are listed in Table 5A-5. It is seen that the out of plane shear and hoop force have changed due to the failure of the hoop tendons. The shear has increased considerably, but, is in the opposite direction of the shear due to aircraft impact, and therefore aids in resisting the aircraft impact. When the aircraft impact diminishes and the hoop tendons are still broken, the remaining shear is much less than the ultimate shear stress according to ACI 318-63.

The above analysis does not consider the moments caused by the loss of 8 hoop tendons. Referring to Figure 5A-34, which is a comparison of (1) the loading due to aircraft impact plus total prestress and (2) the loading due to aircraft impact plus total prestress minus the hoop prestress due to the loss of hoop tendons, it can be deduced that the resulting moments will tend to counteract the moments caused by the aircraft impact. When the aircraft impact diminishes, the axial compression due to the remaining prestress forces (see Table 5A-5) should be sufficient to overcome the tension due to the moments caused by the loss of hoop prestress.

Based on the above logic and conservative numerical calculation, it is believed that the aircraft impact in the direction shown on Figure 5A-33 does not jeopardize the stability of the structure.

#### 4.3 SPALLING DUE TO AIRCRAFT IMPACT ON THE OUTSIDE WALL

Spalling is the kind of fracture which results from the interference between the incident compressional wave and its reflected counter-part. The mechanics of spalling can be described graphically as follows:



Compressive wave before reaching the free surface

Part of the compressive wave reflected back from the free surface



The spalling will occur at a distance  $p$  from the free surface, if the net tensile stress AB exceeds the tensile fracture strength of the material (References 23 and 24). From these we can see that the spalling is influenced by two factors, (a) the duration and shape of the stress pulse, and (b) property of the material acted on.

The plane dilatational wave will travel through the plate at the speed of  $\sqrt{\frac{\lambda + 2\mu}{\rho}}$ , where  $\lambda$ ,  $\mu$  are Lamé's constants and  $\rho$  is the density of the material.

Transform  $(\lambda + 2\mu)$  to a form in terms of Young's Modulus  $E$ , and Poisson's ratio  $\nu$ , which engineers are more familiar with. We have:

$$\lambda + 2\mu = \frac{E(1 - \nu)}{(1 + \nu)(1 - 2\nu)}$$

For concrete, with  $E = 4,000$  ksi,  $\nu = 0.15$ ,  $\rho = 145$  lb/ft<sup>3</sup>, the wave velocity is:

$$c = 1.4 \times 10^5 \text{ in./sec} = 11,650 \text{ ft/sec.}$$

Hence, for the structure we are concerned with, the spalling may occur only for the stress pulse duration of the order of microseconds. The first unloading of our impact force occurs at 0.19 seconds. In other words, for a wall of 5 ft thickness, the wave has to travel back and forth almost 220 times before the impact force reaches the unloading point. Due to the internal friction, the stress wave is long dispersed before it can build up tensile stress in the structure. So the spalling effect is almost impossible to occur.

Nevertheless, the anchors on the containment vessel liner above grade will be deeply anchored into the concrete wall with one inch diameter bolts (form ties). These bolts have a capacity to resist 1.7 kips per foot of anchor. This measure further protects the liner anchors against failure due to spalling; even though such behavior is not anticipated, as previously described.

The design criteria for the liner anchors is described in Section 5.2.3.2.5 "Liner Anchor". The liner angle welds have been tested by 20 percent liquid penetrant test 100 visual inspection in accordance with the requirements of Section VIII of ASME Boiler and Pressure Vessel Code. Three specimens of the liner angle welds were tested by Pittsburgh Testing Laboratory and the factor of safety was found to be 2.7 against the worst possible load on the liner anchor.

#### 4.4 IMPACT EFFECTS ON EQUIPMENT AND COMPONENTS

To eliminate the shock effect caused by an aircraft impact, the concrete floor slabs in the Control Building have been separated by a 2 inch wide joint from the exterior walls exposed to an aircraft impact. The concrete slabs are supported by steel beams which in turn are supported on elastomeric pads which act as vibration dampeners.

4.5 REFERENCES

1. Haley, Jr., J. and Turnbow, J., "Total Reaction Force due to an Aircraft Impact into a Rigid Barrier," AvSER Report prepared for Gilbert Associates, Inc. by Dynamic Science, Phoenix, Arizona, April 1968.
2. Biggs, J. M., "Introduction to Structural Dynamics," McGraw-Hill Book Co., N.Y. 1964, Section 2.3.
3. J. Martin, "Impulsive Loading Theorem For Rigid-Plastic Continua," J. Engineering Mechs. Div., ASCE, EM5, October 1964, pp. 27-42.
4. K. Forsberg and W. Flugge, "Point Load On a Shallow Elliptic Paraboloid," To Appear in Journal of Applied Mechanics.
5. A. Kalnins and P.M. Naghdi, "Propagation of Axisymmetric Waves in An Unlimited Elastic Shell," Journal of Applied Mechanics, 27, 1960, pp 690-695.
6. C. H. Norris 'et al': "Structural Design for Dynamic Loads," McGraw Hill, 1959.
7. J. N. Cernica and M. J. Charignon: "Ultimate Static and Impulse Loading of Reinforced Concrete Beams." ACI Journal, V. 50, No. 9, 1963, pp. 1219-1228
8. Walter Cowell: "Dynamic Properties of Plain Portland Cement Concrete." Naval Civil Engin. Lab., Port Huenema, Calif. Report NCEL 447, 1966.
9. H. Weigler and G. Becker: "Der Bauingenieur," Berlin, Vol. 36, No. 10, 1961, pp. 390-396.
10. J. Peter: "Zur Bewehrung von Scheiben und Schalen fur Hauptspannungen Schiefwinklig zur Bewehrungstrichtung," Doctoral Thesis, Technische Hochschule Stuttgart, 1964.
11. G. W. D. Vile: "Strength of Concrete Under Short-Time Static Biaxial Stress." Proceedings of International Conference on Structural Concrete, London, 1965.
12. Fritz Leonhardt: "Prestressed Concrete Design and Construction" Wilhelm Ernst & Sohn, 1964, pp. 59.
13. Volterra, E. and Zachmanoglou, E., "Dynamics of Vibrations," Charles Merrill Books, Inc., Columbus, Ohio, 1965.
14. Timoshenko, S. and Young, D., "Vibration Problems in Engineering," 3rd Ed., D. Van Nostrand Co., Inc., 1955.

15. Harris, C. and Crede, C., "Shock and Vibration Handbook," McGraw-Hill Book Co., N.Y., 1961.
16. Bogner, F., Fox, R., and Schmit, L., "The Generation of Interelement-Compatible Stiffness and Mass Matrices by the Use of Interpolation Formulae," Proc. Conf on Matrix Methods in Structural Mech., Dayton, Ohio, 1965.
17. Gallagher, R., "The Development and Evaluation of Matrix Methods for Thin Shell Structural Analysis," Ph.D. Dissertation, State University of New York at Buffalo, 1966.
18. Gallagher, R. and Yang H., "Elastic Instability Prediction of Doubly Curved Shell Structures," 2nd conference on Matrix Methods in Structural Mechanics, Wright-Patterson Air Force Base, Dayton, Ohio, Oct. 1968.
19. Yang, H., "A Finite-Element Formulation for the Instability Prediction of Doubly Curved Shell Structures," Ph.D. Dissertation, Cornell University, Ithaca, N.Y., Oct. 1968.
20. Timoshenko, S. and Goodier, J. N., "Theory of Elasticity," McGraw-Hill Book Co., 1951.
21. Riera, J. D., "On the Stress Analysis of Structures Subjected to Aircraft Impact Forces", Nuclear Engineering and Design, August, 1968.
22. Gwaltney, R. C., "Missile Generation and Protection in Light-Water-Cooled Power Reactor Plants" U.S. Atomic Energy Commission, DRNL-NSIC-22, September, 1968.
23. Rinehart, John S. and Pearson, John, "Behavior of Metals under Impulsive Loads" Dover, 1965.
24. Kolsky, H. "Stress Waves," Dover, 1963.
25. Wood, R. H. "Plastic and Elastic Design of Slabs and Plates," Ronald, 1961.
26. Rosenthal, I. and Glucklich, J., "Strength of Plain Concrete under Biaxial Stress," ACI Journal, November 1970.